Earth and Planetary Science Letters 512 (2019) 111–123

Contents lists available at ScienceDirect

Earth and Planetary Science Letters

www.elsevier.com/locate/epsl

Grain-size-dependent remanence anisotropy and its implications for paleodirections and paleointensities – Proposing a new approach to anisotropy corrections

Andrea R. Biedermann [a,*], Dario Bilardello [a], Mike Jackson [a], Lisa Tauxe [b], Joshua M. Feinberg [a]

[a] Institute for Rock Magnetism, University of Minnesota, 116 Church St SE, Minneapolis, MN 55455, USA
[b] Scripps Institution of Oceanography, University of California, San Diego, 9500 Gilman Dr, La Jolla, CA 92093, USA

ARTICLE INFO

Article history:
Received 15 March 2018
Received in revised form 7 January 2019
Accepted 28 January 2019
Available online 18 February 2019
Editor: B. Buffett

Keywords:
paleomagnetism
remanence anisotropy
anisotropy correction
paleodirection
paleointensity
Bushveld Complex

ABSTRACT

Paleomagnetic data provide information on the evolution of the Earth's magnetic field, and are used to reconstruct plate motions. One fundamental assumption underlying these interpretations is that the magnetization of a rock reliably records the direction and intensity of the magnetizing field, i.e. that the magnetization is parallel to the field direction, and the intensity of magnetization is proportional to the field strength. Preferred alignment or anisotropic distribution of magnetic grains can affect both the direction and the intensity of magnetization. Therefore, correction techniques, employing the anisotropy of magnetic susceptibility (AMS), thermal remanence (ATRM), or anhysteretic remanence (AARM) are used to account for these effects. We find that AARM within the same rock can vary dramatically with coercivity/grain size, so that anisotropy corrections can also depend on how AARM was measured.

A consequence of the dependence of AARM on coercivity is that although a specimen may have been magnetized in a single direction, different grain size fractions may record magnetizations in different orientations. These directional variations, as revealed during progressive alternating field (AF) demagnetization, could erroneously be interpreted as changes in field or reorientation of the rock unit, when in reality they are related to grain-size-dependent remanence anisotropy. Similarly, intensity variations caused by grain-size-dependent anisotropy may bias paleointensity estimates. These observations have important consequences for studies on the evolution of the Earth's magnetic field, magnetic overprinting, and paleogeographic reconstructions.

1. Introduction

Reliable paleomagnetic data, i.e. paleomagnetic directions and paleointensities, are essential for (1) describing the past evolution of the Earth's magnetic field which in turn helps understand the geodynamo and forms the basis for archeomagnetic dating, and (2) for paleogeographic reconstructions. Paleointensity data are used to characterize the processes related to magnetic field reversals or the absence of such reversals (superchrons), and paleosecular variation (Biggin et al., 2012; Prévot et al., 1985; Tarduno et al., 2006; Tauxe and Yamazaki, 2015), date archeological materials (Ben-Yosef et al., 2010; Stillinger et al., 2016), estimate the onset of inner core growth (Biggin et al., 2015; Buffett, 2003; Hale, 1987; Tarduno et al., 2006), or determine whether extraterrestrial bodies also possess geodynamos (Cisowski et al., 1983). Directional data provide information for paleogeographic reconstructions of plate configurations (Dietz and Holden, 1970; Hospers and van Andel, 1969; Irving, 1957; Morel and Irving, 1981), and help evaluate the symmetry and dipole- versus non-dipole components of the field (Evans, 1976; Pesonen and Nevanlinna, 1981; Swanson-Hysell et al., 2009; Tauxe and Kent, 2004; van der Voo and Torsvik, 2001).

Two fundamental assumptions in paleomagnetic and paleointensity studies are that (1) the magnetization is parallel to the inducing field, and (2) the intensity of the magnetization is proportional to the field. Some of the challenges in obtaining and interpreting paleomagnetic data include the non-continuity of the record, alteration and remagnetization of rocks (Dunlop et al., 1997; Elmore et al., 2012), limited stability of magnetic grains (Levi, 1977), cooling rate effects (Bowles et al., 2005; Walton, 1980; Yu, 2011), a non-linear relationship between field strength and

* Corresponding author. Now at: Institute of Geological Sciences, University of Bern, Baltzerstrasse 1+3, 3012 Bern, Switzerland.
E-mail address: andrea.regina.biedermann@gmail.com (A.R. Biedermann).

https://doi.org/10.1016/j.epsl.2019.01.051
0012-821X/

thermal remanence (Coe, 1967; Selkin et al., 2007), low-field bias in paleointensity data (Smirnov et al., 2017) and anisotropy (Rogers et al., 1979; Kent and Irving, 2010; Selkin et al., 2000). Paleomagnetic studies on magnetic inclusions within silicates have been successful in overcoming some of these issues, because these magnetic inclusions are protected against alteration by their host silicates, and because they are confined to a certain size range (Cottrell and Tarduno, 1999; Feinberg et al., 2005; Tarduno et al., 2006; Selkin et al., 2008). However, one potential problem with such inclusions is that they generally have a preferred orientation with respect to the silicate lattice, resulting in anisotropic remanence acquisition if the silicates are aligned (Feinberg et al., 2006).

Remanence anisotropy affects both the direction and intensity of magnetization acquired, with important consequences for inferred apparent polar wander paths, paleogeographic reconstructions, or paleointensity studies. One of the simplest ways to correct for these effects is by measuring anisotropy of magnetic susceptibility (AMS) and multiplying the observed magnetization vector with the inverse of the AMS tensor, i.e. because $\vec{M} = \boldsymbol{k} * \vec{H}$, it follows that $\vec{H} = inv(\boldsymbol{k}) * \vec{M}$. However, AMS represents a superposition of paramagnetic, diamagnetic and ferromagnetic contributions, making it unrepresentative of remanence anisotropy, and has been described as inadequate for detecting paleofield deflections in paleomagnetism (Selkin et al., 2000), archeomagnetism (Borradaile et al., 2001; Tema, 2009), and extraterrestrial magnetism (Gattacceca et al., 2003). Anisotropy of thermal, anhysteretic, or isothermal remanent magnetization (ATRM, AARM, and AIRM) are more direct representations of the anisotropy of remanence carrying grains. Because of possible alteration during thermal experiments, AARM is often preferred to assess remanence anisotropy (Potter, 2004), and Mitra et al. (2013) demonstrated that AARM and ATRM corrections can give comparable results for some specimens. But, care has to be taken when the remanence is carried by grains other than single domain magnetite for which Néel theory applies, because coercivities cannot be easily related directly to blocking temperatures. If several different minerals contribute to the natural remanent magnetization (NRM) or the remanence anisotropy, the magnetization of each mineral needs to be corrected with its own specific anisotropy (Borradaile and Almqvist, 2008; Kodama and Dekkers, 2004). For example, inclination shallowing in sediments should be corrected with the remanence anisotropy of the grain population carrying the characteristic remanence (Kodama, 1997, 2012).

Similarly, if subpopulations of the same mineral but different grain sizes possess different anisotropies, one would expect that the remanence carried by each subpopulation would be affected by its own anisotropy. It has been demonstrated that the preferred alignment of distinct sub-populations of magnetite grains can be characterized by measuring the anisotropy of partial ARMs (ApARMs) (Jackson et al., 1988). A number of studies have since used ApARMs to capture the remanence anisotropies of specific grain sizes to describe primary vs secondary fabrics, or differences in fabrics recorded by different grain sizes (Aubourg and Robion, 2002; Bilardello and Jackson, 2014; Trindade et al., 1999). Even though these studies illustrate that ApARMs in the same rock can vary dramatically with grain size or coercivity window, most studies still measure AARMs by imparting a remanence in the 0–100 mT AF range, thus measuring an averaged anisotropy over all the coercivity windows in the specimen.

Remanence anisotropy varies with coercivity in a large variety of specimens with multiple remanence carriers. This calls for a more complete assessment of how changes in remanence anisotropy with grain size affect magnetization direction and intensity, and relevant implications for anisotropy corrections. In this study, we measured a series of ApARM tensors and their thermal analogs, anisotropy of partial TRMs (ApTRM) tensors for selected specimens of the Bushveld Complex from South Africa. While our ApTRM experiments have been inconclusive, we will show how ApARM tensors within the same specimen can change among low, intermediate and high coercivity windows, and how these ApARM tensors compare to the AARM tensors measured over typical coercivity ranges used in AARM experiments. Each of these A(p)ARM tensors can be used to predict how much the intensity and direction of the magnetization would differ from that observed in an isotropic specimen for any given field direction. These predictions represent the expected uncertainty in paleodirection and paleointensity estimates, and how these vary with the coercivity fraction of the remanence-carrying grains. To illustrate how grainsize-dependent remanence anisotropy may affect NRM acquisition, we investigate the direction of an ARM imparted along the specimen z-axis (randomly oriented with respect to the anisotropy principal axes), with a special focus on changes in magnetization direction during AF demagnetization and acquisition of an ARM. This experiment underlines how for a given field direction, the magnetization direction in the same specimen can change according to variations in the A(p)ARM tensor with coercivity/grain size.

Based on these investigations, we develop a conceptual model for anisotropic remanence acquisition in rocks with complex fabrics, and propose a new procedure for anisotropy corrections. In particular, we suggest that (1) ApARMs are measured for different coercivity windows to capture the specific anisotropies of grain subpopulations, (2) a combination of ApARM tensors determined in multiple coercivity windows that together carry the characteristic remanence is used for anisotropy corrections, and (3) the directional data of ARM demagnetization or ARM acquisition experiments is also examined, in order to provide a first measure of how strongly remanence anisotropy varies with grainsize. These findings are broadly applicable to TRMs and ARMs, and as other researchers have noted in the past, single particle anisotropy must be taken into account when this approach is used for depositional remanence anisotropy (e.g. Jackson et al., 1991; Kodama, 2012).

2. Materials

Specimens used in this study are gabbronorites from the Bushveld Complex, South Africa, with preferred orientation of pyroxene, plagioclase, and remanence-carrying grains within these silicates (Feinberg et al., 2006). Several existing paleomagnetic studies on rocks from the Bushveld Complex report paleopoles with considerable spread, which has been attributed to differences in emplacement ages and/or post-emplacement deformation related to re-equilibration of isostasy (Hattingh, 1986; Letts et al., 2009, and references therein). Because anisotropy affects magnetization directions and neither of these studies corrected for these effects, anisotropic remanence acquisition could provide another possible explanation. The remanence of the Bushveld specimens used in this study is held primarily by low-Ti magnetite inclusions exsolved in silicates, such as pyroxene and plagioclase, along with rare pyrrhotite (Feinberg et al., 2006). We have measured ApARMs and AARMs on eight specimens, followed by A(p)TRM measurements on a subset of four of these, and compared the new results to directional data from previous paleointensity experiments on 35 of the Bushveld specimens. The original NRM demagnetization patterns for these samples are included in the supplemental information for this paper (Fig. A).

3. Methods

3.1. Paleointensity

Paleointensity experiments followed the IZZI-Thellier protocol (Yu et al., 2004). The specimens were thermally demagnetized

in a laboratory-built, non-inductively wound furnace whose temperature is monitored via three thermocouples and is controlled through a LabView module at the Scripps Institution of Oceanography, UC San Diego, at temperatures up to 550 °C. Partial thermal remanences (pTRMs) were imparted parallel to the specimen z-axes in a field of 20 μT during cooling. For this study, we were mainly interested in the direction of the imposed pTRM at every temperature step. This magnetization was calculated as a vector difference between the demagnetized and the magnetized states for the same temperature.

3.2. Remanence anisotropy

TRM and pTRM anisotropies were characterized by applying a 50 μT field while specimens were cooling from 600 °C to room temperature in an ASC-Scientific TD48SC furnace. Subsequently, all specimens were demagnetized to 500 °C, then to 550 °C, in order to determine the $ApTRM_{500-600}$ and $ApTRM_{550-600}$. After each step, TRMs were measured on a 2G Enterprises 760-R SQUID superconducting rock magnetometer (SRM). This procedure was repeated for three directions (x, y and z) on a thermally demagnetized specimen, followed by a full TRM along the x-axis, in order to check for specimen alteration. The difference between the first and second measurement of the full TRM parallel to x should be distinctly smaller than the differences between the full TRMs acquired parallel to the x, y, and z axes that are related to anisotropy. TRM anisotropy tensors were calculated from the full-vector magnetizations.

A series of seven ApARM/AARM tensors was determined for each specimen, using coercivity windows of 0–20, 20–50, 50–100, 100–180, and 0–50, 0–100, 0–180 mT. The former series will be referred to as ApARMs (e.g., $ApARM_{20-50}$), and the latter as AARMs (e.g., $AARM_{0-50}$) throughout this paper. For each dataset, a 0.1 mT DC field was applied on a DTech D-2000 AF demagnetizer in the respective AF demagnetization interval. Decay rates varied from 0.0001 mT/half-cycle for AF $\leq$ 5 mT, to 0.0075 mT/half-cycle at 200 mT AF. The remanence was subsequently measured on the 2G-760 SRM. The procedure was repeated for 9 orientations, and specimens were demagnetized to 200 mT AF in-between steps. ApARM and AARM remanence susceptibility tensors were then computed using the field-parallel remanence components, $M_{\parallel} = \vec{M} \cdot \boldsymbol{k}\vec{H}/|\vec{H}|$, analogous to the conventional method for AMS calculation.

All remanence anisotropy tensors are characterized by their eigenvalues ($k_1 \geq k_2 \geq k_3$) and eigenvectors, the mean (p)ARM or (p)TRM $k_{mean} = (k_1 + k_2 + k_3)/3$, the anisotropy degree $P = k_1/k_3$ or $k' = \sqrt{((k_1 - k_{mean})^2 + (k_2 - k_{mean})^2 + (k_3 - k_{mean})^2)/3}$, and the shape $U = (2*k_2 - k_1 - k_3)/(k_1 - k_3)$. U varies from -1 for uniaxial rotationally symmetric prolate ellipsoids to $+1$ for uniaxial oblate ones, and we will use the more general terms 'oblate' and 'prolate' to describe triaxial fabrics with $0 < U < 1$ and $-1 < U < 0$, respectively. Hext (1963) statistics, i.e. confidence ellipses and F-tests, was used to determine whether a specimen possesses a significant anisotropy in each coercivity or temperature window, and whether principal directions of different windows are distinct at the 95% confidence level.

3.3. Effects of magnetic anisotropy on remanence acquisition

To investigate the anisotropy-related NRM deflections and intensity variations including their dependence on coercivity, the magnetization vector, $\vec{M} = \boldsymbol{k}\vec{H}$ was compared to the intensity of magnetization, $M = k_{mean}H$, and the direction of the inducing field, $\vec{H}$. For each ApARM and AARM tensor, the expected angular deviations were computed for all possible field orientations as the acute angle between $\vec{M}$ and $\vec{H}$, and the corresponding intensity deviations by $|\vec{M}|/M$.

Finally, specimens were given an ARM parallel to the specimen z-axis in a 0.1 mT DC field applied over 0–200 mT AF. This ARM, imparted to represent an NRM acquired in a constant field, was subsequently stepwise AF demagnetized (steps of 2, 5, 10, 15, 20, 30, 40, 50, 60, 70, 80, 90, 100, 120, 140, 160, 180, 200 mT). Intensity and direction of the remaining remanence were measured after each demagnetization step. After demagnetization to 200 mT, a new ARM, again parallel to z, was stepwise imposed on the specimen using the same steps as for the demagnetization, again measuring the remanence direction as well as intensity after each step. The resulting remanence direction during AF demagnetization and ARM acquisition was then compared to the known field direction. The field intensity, calculated from the magnetization and A(p)ARM tensors was compared to the known intensity of the applied DC field. Because this experiment is prone to uncertainties caused by slight changes in specimen orientation each time the specimen is inserted in the magnetometer, the same experiment was repeated on a 2G model 755 SRM with an in-line ARM/AF system, assuring that specimens remained immobile during the entire AF demagnetization or acquisition of ARM. Because the in-line system can only reach 170 mT, the steps for these experiments were 2, 5, 10, 15, 20, 30, 40, 50, 60, 70, 80, 90, 100, 120, 140, 160, 170 mT. The decay rates for the in-line ARM/AF system are related to the speed at which specimens move (15 cm/s) and are thus different for each field. Note that the arbitrary choice of field orientation implies that the ARM direction may be close to a principal axis of one or all the ApARM tensors, resulting in little or no deflection even in anisotropic specimens. Hence, this experiment is an easy way to show that anisotropy is present if a deflection is detected. However, it cannot be used to rule out the presence of anisotropy entirely if no deflection is observed.

4. Results

4.1. Directions of pTRMs acquired during paleointensity experiments

The directions of pTRMs acquired during the paleointensity experiments are dispersed around the field direction. The angle between magnetization and field orientations is generally larger at lower temperatures than at higher temperatures, ranging from sub-parallel to the applied field to nearly perpendicular to the field. In addition, there appears to be a systematic deflection away from the laboratory field at most temperatures for some of the specimens (Fig. 1).

4.2. TRM anisotropy

Three out of four specimens show differences between the first and second set of TRMs acquired parallel to x. The difference, defined by $\Delta M_x = (M_{x,alteration\ check} - M_{x,initial})/M_{x,initial}$, are between -5.6 and $+15.8\%$. In addition, it appears that the TRM acquired along one direction does not fully remagnetize when applying a perpendicular TRM. From these two observations we conclude that (1) specimens may have chemically altered during the experiment, and/or (2) the Thellier Laws of reciprocity and independence do not hold for these specimens. For one specimen, BG2.09a, ΔM_x equals -0.2%. This is the only specimen for which (p)TRM anisotropy will be reported (Table A, online supplementary). Fig. 2 shows that the maximum ATRM axes of all three tensors coincide. There seems to be a rotation of the minimum and intermediate axes from $ATRM_{0-600}$ to $ApTRM_{500-600}$ to $ApTRM_{550-600}$; however, this change in direction is not statistically significant due to the large e_{23} confidence angle. The degree of

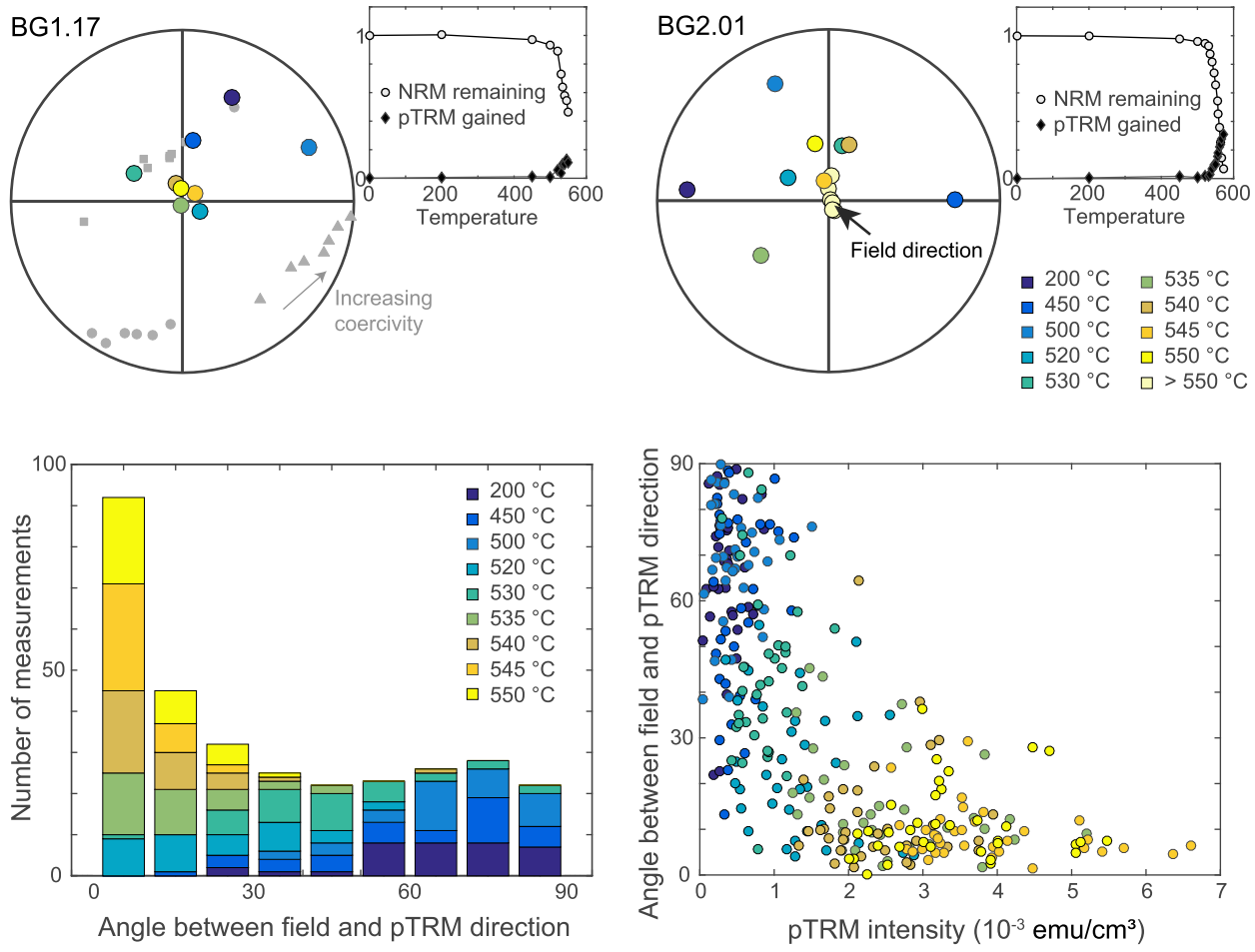

Fig. 1. (Top) Stereoplots showing directions of pTRMs for two specimens acquired during paleointensity experiments; colors indicate temperature. Insets show NRM remaining and pTRM gained for each specimen, with all magnetizations normalized to the initial NRM. For BG1.17, A(p)ARM principal-axis orientations of sister specimen BG1.17a are also shown (grey circles, triangles and squares respectively for minimum, intermediate and maximum axes). (Bottom) Histogram shows pTRM angular deflections (10° bins) for 35 specimens measured at 9 temperatures each. (For interpretation of the colors in the figure(s), the reader is referred to the web version of this article.)

anisotropy increases with increasing lower temperature of the ApTRM window.

4.3. ApARM and AARM tensors and effect on remanence direction and intensity

All specimens acquire ARMs, and these are generally anisotropic (Online Supplementary Tables B (summary) and C (all data)). Three specimens do not display significant anisotropy in the 0–20 mT AF window, where the mean ARM is lowest, and three samples have insignificant anisotropy in the 0–50 mT AF window, as defined by e_{13} confidence angles $> 26°$ and $F > 9.01$ (Hext, 1963). For those tensors with significant AARM, the anisotropy degrees k' and P vary between $1.07 * 10^{-7}$ m^3/kg – $4.64 * 10^{-6}$ m^3/kg, and 1.12–1.59, respectively. For some ApARMs and AARMs in some specimens, the k_2 and k_3 values cannot be distinguished at 95% confidence, as indicated by $F_{23} < 9.55$ and large e_{23} confidence angles. The shape of the ARM anisotropy varies from $U = -0.92$ to $U = 0.46$. Fig. 3 shows the mean ARM, anisotropy parameters and principal directions for each of the ApARM and AARM tensors for three representative specimens. The $ApARM_{0-20}$ has the weakest mean ARM, and also the weakest k'. Compared to the other ApARMs, $ApARM_{50-100}$ has the highest k', which also dominates the combined AARMs, $AARM_{0-100}$ and $AARM_{0-180}$. The mean ARM, on the other hand, can be higher for $AARM_{100-180}$ than for $AARM_{50-100}$. These observations indicate that although the grains in the higher coercivity window possess higher overall remanence, owing to concentration and/or spontaneous magnetization, they have lower anisotropy than those in the 50–100 mT window.

The principal axes of several or all A(p)ARM tensors in the same specimen can have similar orientations; however, they can also be dramatically different. In particular, the orientation of principal axes can be significantly different for $AARM_{0-20}$ as compared to any of the other ApARMs or AARMs, i.e. the 95% confidence ellipses do not overlap. The other ApARMs and AARMs show similar maximum principal axes directions (overlapping confidence ellipses), however, the intermediate and minimum principal axes appear to rotate with increasing coercivity (non-overlapping confidence ellipses). These differences in principal axes orientations and degree and shape of anisotropy will result in different remanence deflections and intensity changes for the grain populations in each of the coercivity windows, as defined by their AARM and ApARM tensors (Fig. 4).

4.4. Remanence direction for ARM parallel to z

To model a NRM acquired in constant field conditions, and in the absence of any remagnetization or alteration events, an ARM of known intensity and orientation was applied to each specimen. Successive stepwise demagnetization of this ARM shows that (1) the ARM direction generally deviates from the direction of the applied field, and (2) there appears to be a variation of directions with demagnetization step, resulting in a seemingly two-component magnetization (Fig. 5). In a typical paleomagnetic

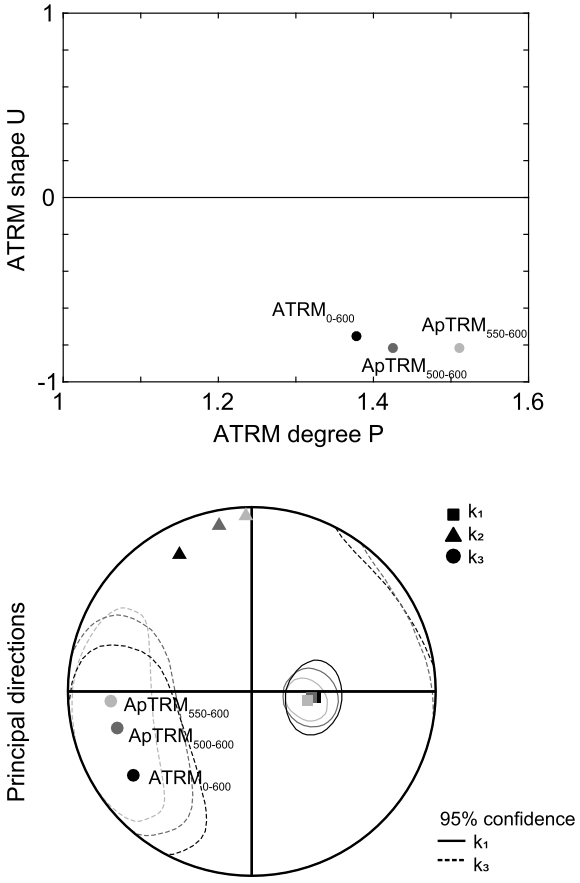

Fig. 2. Anisotropy degree P, shape U and principal directions for the three A(p)TRM tensors of specimen BG2.09a. Note that the directions are not well defined, so that the apparent rotation of minimum and intermediate principal axes with temperature is not significant.

study, the vector endpoint diagrams as shown in Fig. 5 would likely be interpreted as 2 components of magnetization acquired at different times. However, in this study the entire magnetization was acquired in a single magnetization event, with a field of constant orientation. Hence, only the coercivity- and grainsize-dependence of the AARM as shown in Section 4.2 can account for the apparent two-component magnetizations. Similar observations are made during the stepwise acquisition of an ARM in a known field with constant orientation.

To determine whether the directions of ARM remaining or acquired in each coercivity window are significantly distinct or share a common mean orientation, they were separated into groups as defined by the AF 0–20 mT (Group 1), 20–50 mT (Group 2), 50–100 mT (Group 3), and 100–200 mT (Group 4) ranges, for both ARM demagnetization and ARM acquisition of each specimen. Note that in doing so, the directions at 20 mT, 50 mT, and 100 mT were each included in two of the sub-groups. Watson's (1983) common mean test was used to assess if the magnetization vectors of two adjacent subgroups have common or different directions (Table 1). Whereas some sub-groups may share a common mean, most subgroups have different mean directions at the 95% confidence limit.

5. Discussion

5.1. New protocol for anisotropy corrections

Magnetic remanence vectors are commonly corrected for anisotropy using a single AMS, AARM, ATRM or AIRM tensor, and multiplying the magnetization vector with the inverse of this tensor (adjusted for single particle anisotropy in the case of depositional remanence) (Jackson et al., 1991; Kodama, 2012; Selkin et al., 2000). Doing so corrects the overall remanence for the integrated fabric of all remanence-carrying grains, and works well in rocks with a single remanence carrier which also carries the anisotropy. However, care has to be taken when several minerals contribute to the remanence and/or anisotropy, in which case the choice of correct anisotropy tensor is crucial (Bilardello and Kodama, 2010; Selkin et al., 2000).

If an anisotropy correction based on a single tensor were sufficient, correcting the ARM data as shown in Fig. 5 with one adequate remanence anisotropy tensor, would restore an overall, single-component magnetization parallel to the field. However, in rocks with multiple remanence carriers and complex fabrics, different subpopulations of grains may form, alter, and be (re)magnetized at different times. Hence, not all subpopulations of grains will contribute to the characteristic remanence. Likewise, it is possible that several subpopulations of grains combined carry the characteristic remanence, but possess different magnetic fabrics, and upon demagnetization of the NRM it appears as if two (or multiple) components of magnetization are present. No single tensor is able to correct for a seemingly two-component magnetization, because variations in remanence intensity and direction related to coercivity-dependent changes in anisotropy will remain unaccounted for. To account for these effects, we suggest that using a combination of ApARM tensors that reflect the different subpopulations of grains is a more appropriate basis for anisotropy corrections than using a single overarching remanence anisotropy tensor. Alternatively, it is possible that the ATRM tensor is much less affected by differing anisotropies in different partial TRMs and use of that tensor would be preferable. However, most of our specimens show signs of alteration or non-ideal behavior in ATRM experiments, and the principal ATRM and ApTRM directions of the one specimen that did pass the alteration test are ill-defined. Therefore, we can neither confirm nor rule out that ApTRMs are different at this stage, and more work will be needed to investigate the variation of ApTRM with blocking temperature.

To improve the application of AARM, we propose an updated theory of anisotropic remanence acquisition, which takes into account the dependence of anisotropy on coercivity and grain size. For a rock containing multiple subpopulations of grains (sp1, sp2, … spn; assume that sp1 contains the fraction of lowest, and spn the fraction of highest coercivities) with distinct magnetic fabrics ($\boldsymbol{k}_{sp1}$, $\boldsymbol{k}_{sp2} \ldots \boldsymbol{k}_{spn}$), the magnetization it acquires in field $\vec{H}$ is described by $\vec{M}_{tot} = \vec{M}_1 + \vec{M}_2 + \cdots + \vec{M}_n = \boldsymbol{k}_{sp1}\vec{H} + \boldsymbol{k}_{sp2}\vec{H} + \cdots + \boldsymbol{k}_{spn}\vec{H}$. In the general case when $\boldsymbol{k}_{spi}$ is different for each subpopulation, $\vec{M}_1, \vec{M}_2 \ldots \vec{M}_n$, will have different orientations. The anisotropy and remanence of the bulk rock are defined by $\boldsymbol{k}_{tot} = \boldsymbol{k}_{sp1} + \boldsymbol{k}_{sp2} + \cdots + \boldsymbol{k}_{spn}$, and $\vec{M}_{tot}$ (Fig. 6). In a fully magnetized state, the specimen's magnetization is controlled by all subpopulations of grains together, and thus affected by the combination of all $\boldsymbol{k}_{spi}$s. During alternating field demagnetization, it is the lowest-coercivity grains that lose their magnetization first, followed by the intermediate and high-coercivity grains. Similarly, in the case of thermal demagnetization, the lowest unblocking temperatures are removed first, although the relationship between coercivity and blocking temperature is not straight forward except for grains whose magnetizations are carried by uniaxial single domain magnetite and we are discussing only the coercivity-dependence of anisotropy here. The total magnetization is carried by all grains (sp1 … spn). Then after the first demagnetization step the remaining magnetization is carried by sp2 … spn, and so on. The remanence after each step is controlled by the corresponding anisotropies $\boldsymbol{k}_{tot}, \boldsymbol{k}_{sp2} + \cdots + \boldsymbol{k}_{spn}$, and so on. During ARM acquisition, the lowest-coercivity grains are

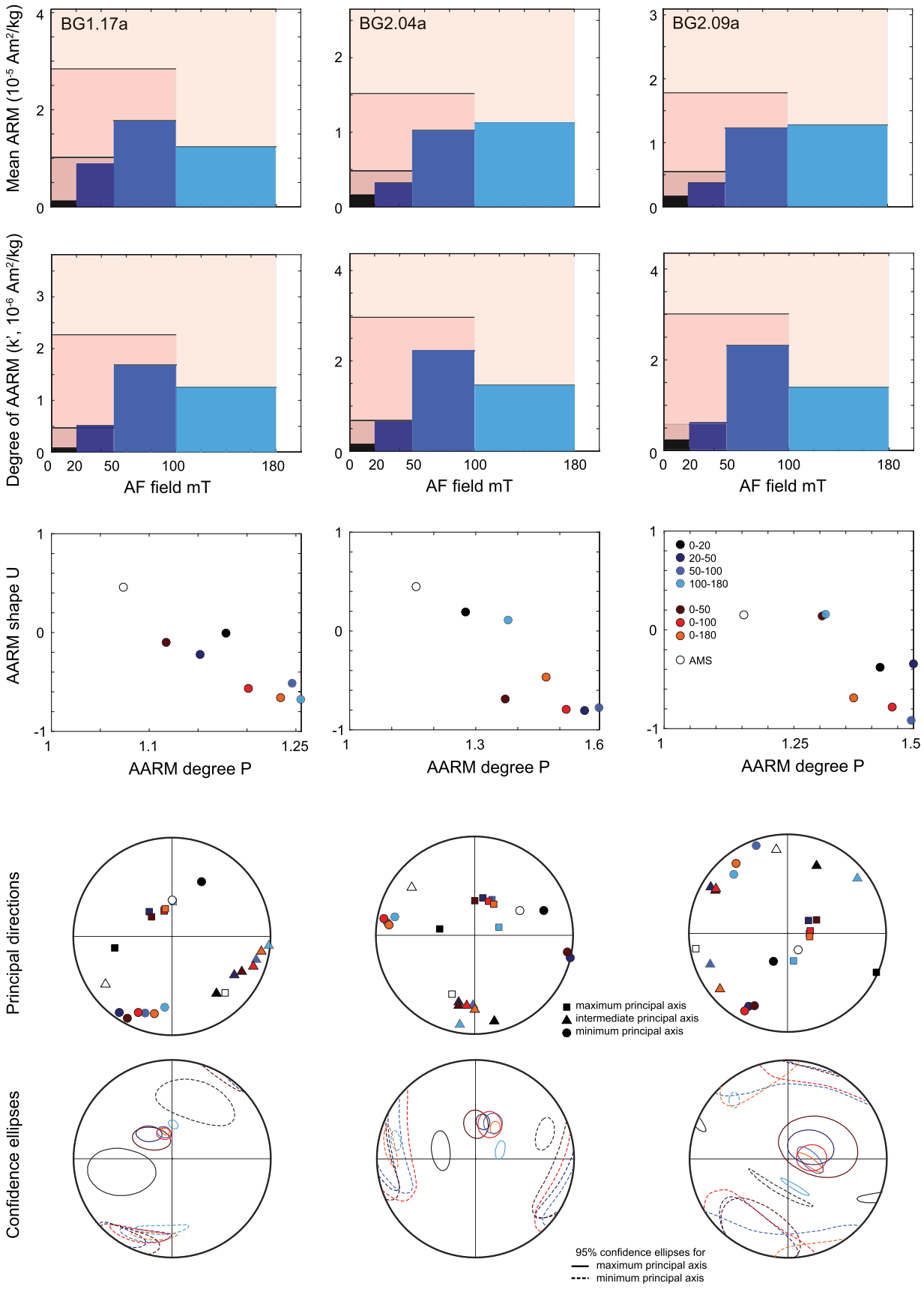

Fig. 3. Mean ARM, k', P, U and principal directions for all ApARM and AARM tensors of each specimen. Blue/black bars are for individual AF windows (ApARMs); pink/tan bars represent AARMs measured over combined windows, i.e. 0–50, 0–100 and 0–180 mT. Note that the window with the highest mean ARM does not necessarily carry the strongest anisotropy, and that the principal axes, degree and shape of anisotropy can vary dramatically between different A(p)ARMs of the same specimen, and do generally not coincide with the respective parameters for AMS.

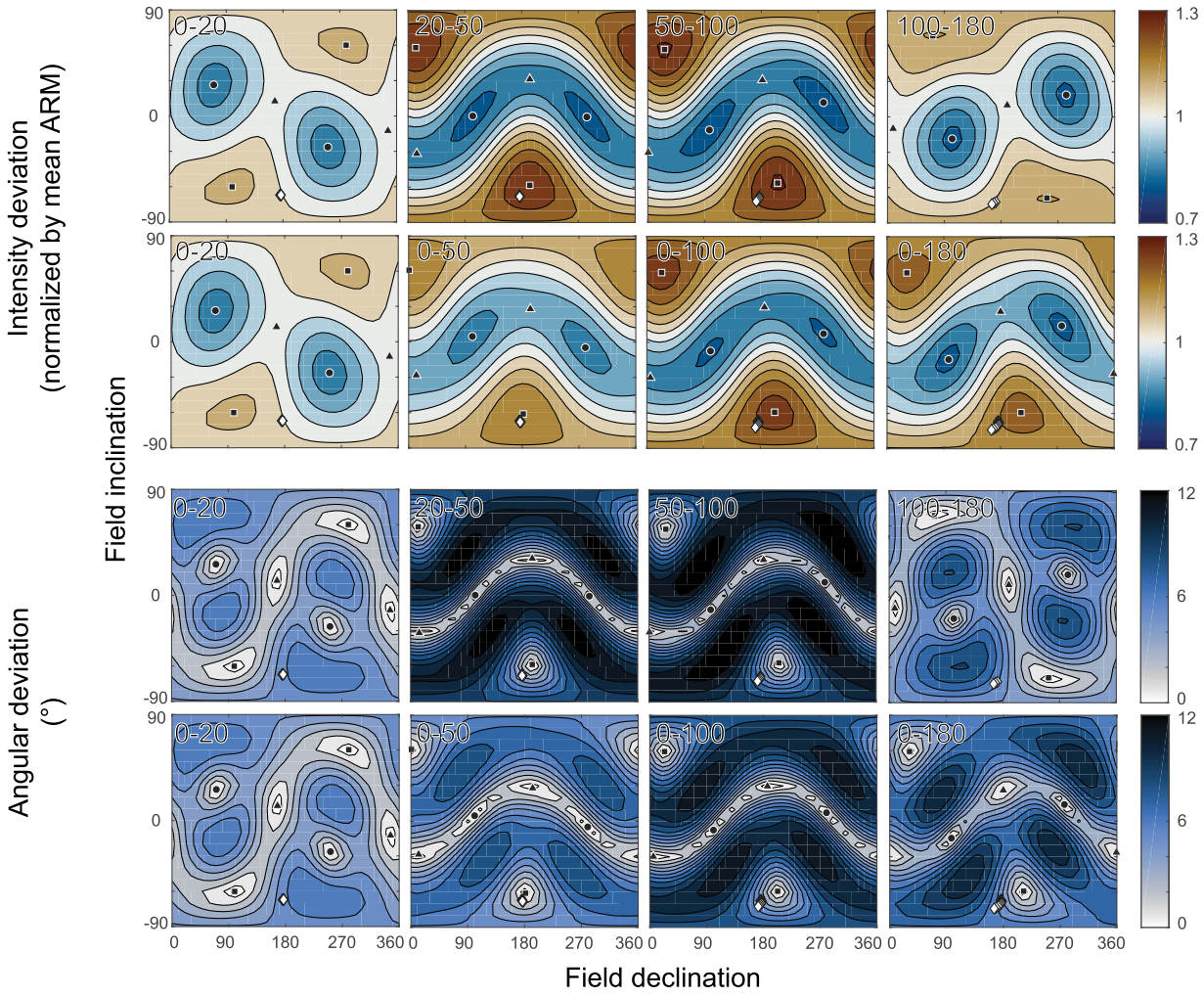

Fig. 4. Angular and intensity deviations for specimen BG2.04a in each coercivity window as compared to an isotropic specimen with the same kmean, magnetized parallel to the field direction, as a function of field declination and field inclination. Each graph represents a different coercivity window, as indicated in the top left (e.g. 0–20 mT). Squares, triangles, and circles indicate the directions of maximum, intermediate and minimum principal A(p)ARM axes for each window, and diamonds indicate the set of natural remanence directions during AF demagnetization in the same window.

Table 1
Watson (1983) test of common means. 'yes' means that the hypothesis that two subgroups have a common mean cannot be rejected at the 95% confidence interval, 'no' means that the two subgroups have different mean directions at the 95% confidence level.

Sample and group	Demagnetization of ARM // z			Acquisition of ARM // z		
	Watson's V	V critical	Common mean?	Watson's V	V critical	Common mean?
BG1.17a						
Group 1 – Group 2	11.1	7.4	no	1.2	8.8	yes
Group 2 – Group 3	15.9	7.3	no	5.7	8.4	yes
Group 3 – Group 4	0.4	8.9	yes	21.3	7.1	no
Group 4 – Group 1	0.4	8.7	yes	0.5	8.7	yes
BG2.04a						
Group 1 – Group 2	3.3	7.1	yes	13.9	8.2	no
Group 2 – Group 3	7.8	7.2	no	14.8	8.0	no
Group 3 – Group 4	14.2	9.3	no	14.6	7.4	no
Group 4 – Group 1	17.1	9.4	no	369.2	7.0	no
BG2.09a						
Group 1 – Group 2	0.1	7.3	yes	1.1	7.5	yes
Group 2 – Group 3	18.9	7.8	no	11.2	7.3	no
Group 3 – Group 4	13.5	8.9	no	21.6	7.5	no
Group 4 – Group 1	20.2	8.8	no	66.3	7.4	no

magnetized first, and the magnetization is affected by $\boldsymbol{k}_{sp1}$. Subsequently, intermediate and then high-coercivity-grains get magnetized, and their anisotropy also starts contributing to the fabric affecting remanence. Thus, the relevant anisotropy is $\boldsymbol{k}_{sp1}$, then $\boldsymbol{k}_{sp1} + \boldsymbol{k}_{sp2}$, $\boldsymbol{k}_{sp1} + \boldsymbol{k}_{sp2} + \boldsymbol{k}_{sp3}, \ldots, \boldsymbol{k}_{sp1} + \cdots + \boldsymbol{k}_{spn}$. Hence, $\vec{H} = inv(\boldsymbol{k}_{tot})\vec{M}_{tot}$ is used to retrieve the field information from the observed $\vec{M}_{tot}$. The tensor and therefore also the correction equation change during the demagnetization: $\vec{M}_i$, the remaining

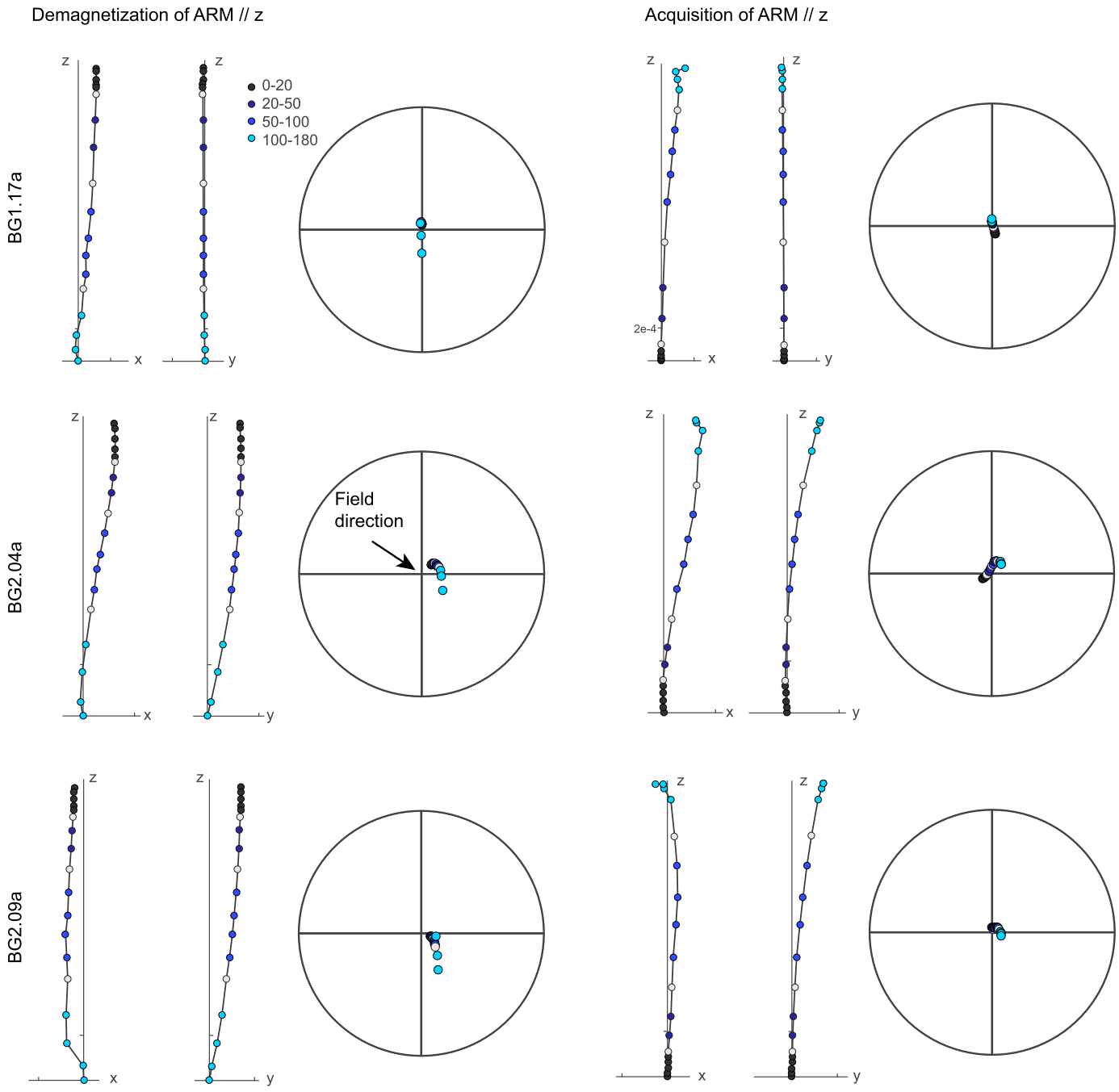

Fig. 5. Demagnetization of an ARM acquired parallel to z in the lab, and acquisition of an ARM parallel to z. Vector endpoint diagrams with equal axes, and stereonets showing the direction of the ARM after each demagnetization or acquisition step. Tick marks in all vector endpoint diagrams are $2 * 10^{-4}$ A m^2/kg.

magnetization after demagnetizing at the alternating field AF_i has to be corrected using

$$\vec{H} = inv(\boldsymbol{k}_{sp(i+1)} + \cdots + \boldsymbol{k}_{spn})\vec{M}_i = inv(\boldsymbol{k}_{tot} - \boldsymbol{k}_{sp1} - \cdots - \boldsymbol{k}_{spi})\vec{M}_i.$$

Analogously,

$$\vec{M}_{c,i} = inv(\frac{\boldsymbol{k}_{sp(i+1)} + \cdots + \boldsymbol{k}_{spn}}{kmean_{sp(i+1)} + \cdots + kmean_{spn}})\vec{M}_i = inv(\frac{\boldsymbol{k}_{tot} - \boldsymbol{k}_{sp1} - \cdots - \boldsymbol{k}_{spi}}{kmean_{tot} - kmean_{sp1} - \cdots - kmean_{spi}})\vec{M}_i$$

is the anisotropy-corrected magnetization vector, where the added tensors are normalized by their mean ARM.

If anisotropy corrections based on these tensors successfully retrieve the field in which the ARM was acquired, both in direction and intensity, they can adequately correct the NRM, provided that ARM is a good proxy for NRM. In principle, the theory presented here can be applied to all rocks, and independent of the type of NRM. However, note that anisotropy corrections for detrital remanent magnetization (DRM) also need to take into account the individual particle anisotropy. The different corrections required for TRM and ARM on the one side, and DRM on the other, are related to the nature of acquisition of each of these remanences: the orientation distribution of remanence-carrying particles remains fixed during both TRM and ARM acquisition, whereas particles rotate during the acquisition of a DRM. Therefore, TRMs or ARMs can be corrected using AARMs and the protocol outlined in this paper, whereas the model would have to be adapted to include individual-particle anisotropies in order to use AARMs to correct a DRM (Jackson et al., 1991; Stephenson et al., 1986).

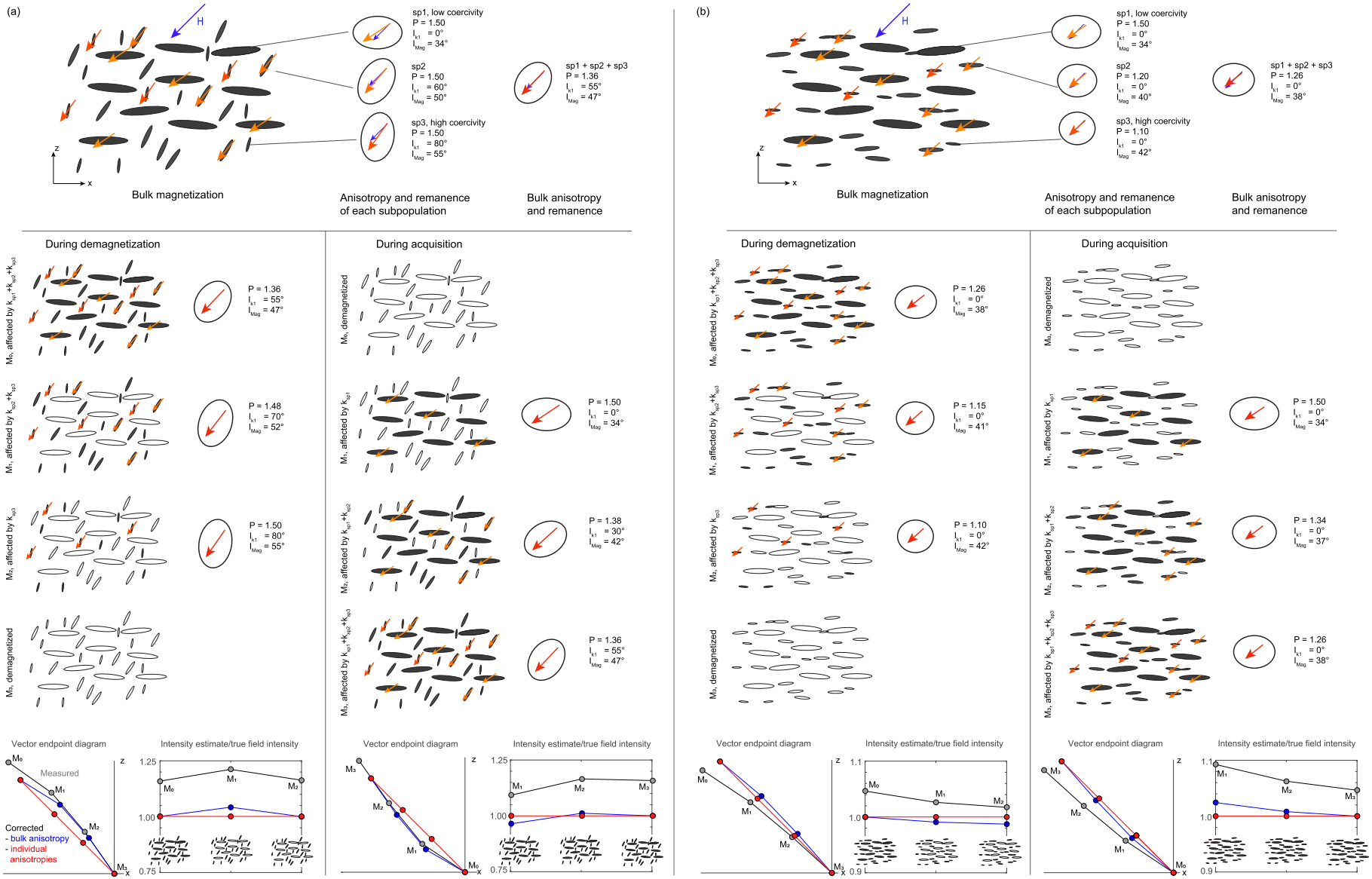

Fig. 6. Conceptual model of remanence acquisition and demagnetization in a rock with several subpopulations of grains with different anisotropies. Filled grains are magnetized, open grains are demagnetized. (a) Shows the effect of variations in fabric orientation with constant degree of anisotropy, and (b) shows the effect of variations in anisotropy degree with constant fabric orientation. H indicates magnetizing field.

Using remanence anisotropy applied over a broad coercivity spectrum will activate the remanence-carrying grains only, in contrast to AMS, which describes the fabric of all grains combined (dia/paramagnetic and ferromagnetic). This leads to a more accurate anisotropy correction, because it more closely reflects the fabric of the grains contributing to the remanence. However, in analogy with complex AMS fabrics, where the anisotropy contributions of different minerals can interfere positively or negatively, the remanence anisotropies of subpopulations of grains with different coercivities can also add constructively or cancel each other out. Therefore, anisotropy corrections should be based on ApARMs rather than AARMs or AMS, to avoid over- or under-correcting the remanence direction and intensity.

Measuring ApARMs in finer coercivity windows theoretically leads to more accurate anisotropy corrections; however, care needs to be taken that windows are not too small, resulting in lower signal-to-noise ratios and consequently not significant fabric results. For each specimen, the windows for ApARM characterization should be chosen such that the fabrics of all subpopulations of grains can be isolated (and corrected for), while making sure that the magnetizations measured in each orientation are strong enough to determine reliable anisotropy tensors. We caution that too large windows may lead to under- or over-corrections of parts of the demagnetization curves, whereas coercivity windows that are too small could lead to no significant anisotropy, or to unrealistically high anisotropy when the noise level is higher than the anisotropy.

A straightforward test for coercivity-dependent changes in anisotropy is to check for changes in the magnetization directions during an ARM demagnetization or ARM acquisition experiment. These changes can be used to determine the optimal coercivity windows in which ApARMs are measured for anisotropy corrections. The same data can also be used to test if anisotropy corrections are successful, because the field direction and intensity are known. ARM demagnetization or acquisition is routinely measured in paleomagnetic studies in order to verify that ARM is an adequate proxy for NRM. For this, the intensity of ARM is compared to that of the NRM during NRM demagnetization. Because the ARM direction is measured as a by-product, these data can be used as a first estimate of anisotropy and changes in anisotropy, by checking (1) whether the ARM is parallel to the field in which it was acquired, and (2) how the ARM direction varies with coercivity. If an ARM is not parallel to the field, this indicates anisotropy, and if its direction varies systematically throughout the ARM demagnetization or ARM acquisition, then this can be related to changes in remanence anisotropy with coercivity. Note that, if the field is applied parallel to one of the principal remanence susceptibility directions, the ARM is parallel to the field even in presence of anisotropy (e.g., Fig. 4). In this case, ARM anisotropy can still be detected if the ARM is imparted along several directions, e.g. x, y, and z, because the intensities will be different. Similarly, the direction of laboratory pTRM acquired in paleointensity experiments can be monitored (as is done in the Thellier GUI program of Shaar and Tauxe (2013)) and checked for anisotropy as well as anisotropy variations with temperature.

5.2. Anisotropy corrections for our specimens

The differences in ApARM tensors indicates that our specimens comprise several subpopulations of remanence carriers, each with a different fabric. Other than for the synthetic model, it is not known *a priori* how many subpopulations there are, which coercivity windows they correspond to, or whether the coercivity windows of two (or several) subpopulations overlap. Further, there were more demagnetization steps in the ARM demagnetization or acquisition experiments than there were coercivity windows for the ApARM measurements. ApARMs were measured for coercivity windows of 0–20, 20–50, 50–100 and 100–180 mT. ARM demagnetization and ARM acquisition was measured in fields of 2, 5, 10, 15, 20, 30, 40, 50, 60, 70, 80, 90, 100, 120, 140, 160, 180, 200 mT on the DTech/2G-760, and 2, 5, 10, 15, 20, 30, 40, 50, 60, 70, 80, 90, 100, 120, 140, 160, 170 mT on the 2G-755. For the demagnetization or acquisition steps at 0, 20, 50, 100 and 180 mT, the combination of ApARMs affecting the remanence and that should be used for the anisotropy correction, corresponds to the findings of the synthetic model. However, for all other steps, it is more complicated. For example, the demagnetization step at 30 mT is affected partly by the ApARM in the 20–50 mT window, as well as the anisotropies carried by higher-coercivity grains, as measured by the ApARMs in higher coercivity windows. This can be expressed as $a * \boldsymbol{k}_{20\text{–}50} + \boldsymbol{k}_{50\text{–}100} + \boldsymbol{k}_{100\text{–}180}$, where the factor a indicates the fraction of the coercivity window involved. The corresponding equation to calculate the field is $\vec{H} = inv(a * \boldsymbol{k}_{sp(i+1)} + \boldsymbol{k}_{sp(i+2)} + \cdots + \boldsymbol{k}_{spn})\vec{M}_i$, and for the anisotropy-corrected magnetization $\vec{M}_{c,i} = inv(\frac{a*\boldsymbol{k}_{sp(i+1)}+\boldsymbol{k}_{sp(i+2)}+\cdots+\boldsymbol{k}_{spn}}{a*kmean_{sp(i+1)}+kmean_{sp(i+2)}+\cdots+kmean_{spn}})$.

Conversely, during acquisition of ARM, the magnetization at 30 mT is affected by the remanence anisotropies of all windows with lower coercivities, as well as the window comprising the 30 mT step; $k_{0\text{–}20} + b * k_{20\text{–}50}$. The coefficients a and b can be approximated by the ratio $kmean_{30\text{–}50}/kmean_{20\text{–}50}$, and $kmean_{20\text{–}30}/kmean_{20\text{–}50}$, i.e. $a = 1 - b$. Assuming that the mean ARM decay or gain is linear in each window, a and b can also be estimated from the fields at which the magnetization is measured, i.e. $a = (50 - 30)/(50 - 20)$ and $b = (30 - 20)/(50 - 20)$. Corrected magnetization directions and field information are thus obtained from $\vec{H} = inv(\boldsymbol{k}_{sp1} + \cdots + \boldsymbol{k}_{sp(i-1)} + b * \boldsymbol{k}_{spi})\vec{M}_i$, and for the anisotropy-corrected magnetization $\vec{M}_{c,i} = inv(\frac{\boldsymbol{k}_{sp1}+\cdots+\boldsymbol{k}_{sp(i-1)}+b*\boldsymbol{k}_{spi}}{kmean_{sp1}+\cdots+kmean_{sp(i-1)}+b*kmean_{spi}})$.

Synthetic 'paleo'directions and 'paleo'intensities were computed from the magnetizations during the demagnetization/acquisition of ARM experiments using different types of anisotropy corrections: (1) isotropic correction with mean ARM susceptibility, (2) anisotropy correction with the $AARM_{0\text{–}100}$ tensor, (3) anisotropy correction with the $AARM_{0\text{–}180}$ tensor, (4) anisotropy correction based on $ApARM_{0\text{–}20}$, $ApARM_{20\text{–}50}$, $ApARM_{50\text{–}100}$ and $ApARM_{100\text{–}180}$, correcting all the measurements between 0–20 mT AF for $ApARM_{20\text{–}180}$, between 20–50 mT AF for $ApARM_{50\text{–}180}$, etc., and (5) anisotropy correction based on $ApARM_{0\text{–}20}$, $ApARM_{20\text{–}50}$, $ApARM_{50\text{–}100}$ and $ApARM_{100\text{–}180}$, correcting the measurements between 0–20 mT AF for the interpolated $ApARM_{20\text{–}180} + a * ApARM_{0\text{–}20}$, etc. Fig. 7 shows vector endpoint diagrams for the demagnetization and acquisition of an ARM parallel to the specimen z-axis before and after correction.

The quality of each correction was assessed by comparing (1) the estimated directions of measured magnetization as well as directions of best-fit lines, and (2) intensities with the known direction and intensity of the field (Fig. 8). For directions, the measures $\sqrt{M_x^2 + M_y^2}$, and $\sqrt{(M_x^2 + M_y^2)/(M_x^2 + M_y^2 + M_z^2)}$ describe how much the measured magnetization deviates from the direction of the field (z) for each specimen and each type of correction. $\sqrt{M_x^2 + M_y^2}$ decreases by about a factor of 2 when anisotropic corrections (2)–(5) are used compared to the mean ARM. In general, there is a slight decrease in $\sqrt{M_x^2 + M_y^2}$ from (2) and (3) to (4) and (5), however, this is small compared to the difference between isotropic and (any) anisotropic correction. While the measure $\sqrt{(M_x^2 + M_y^2)/(M_x^2 + M_y^2 + M_z^2)}$ generally decreases when anisotropy-corrected, it may be larger after correction with

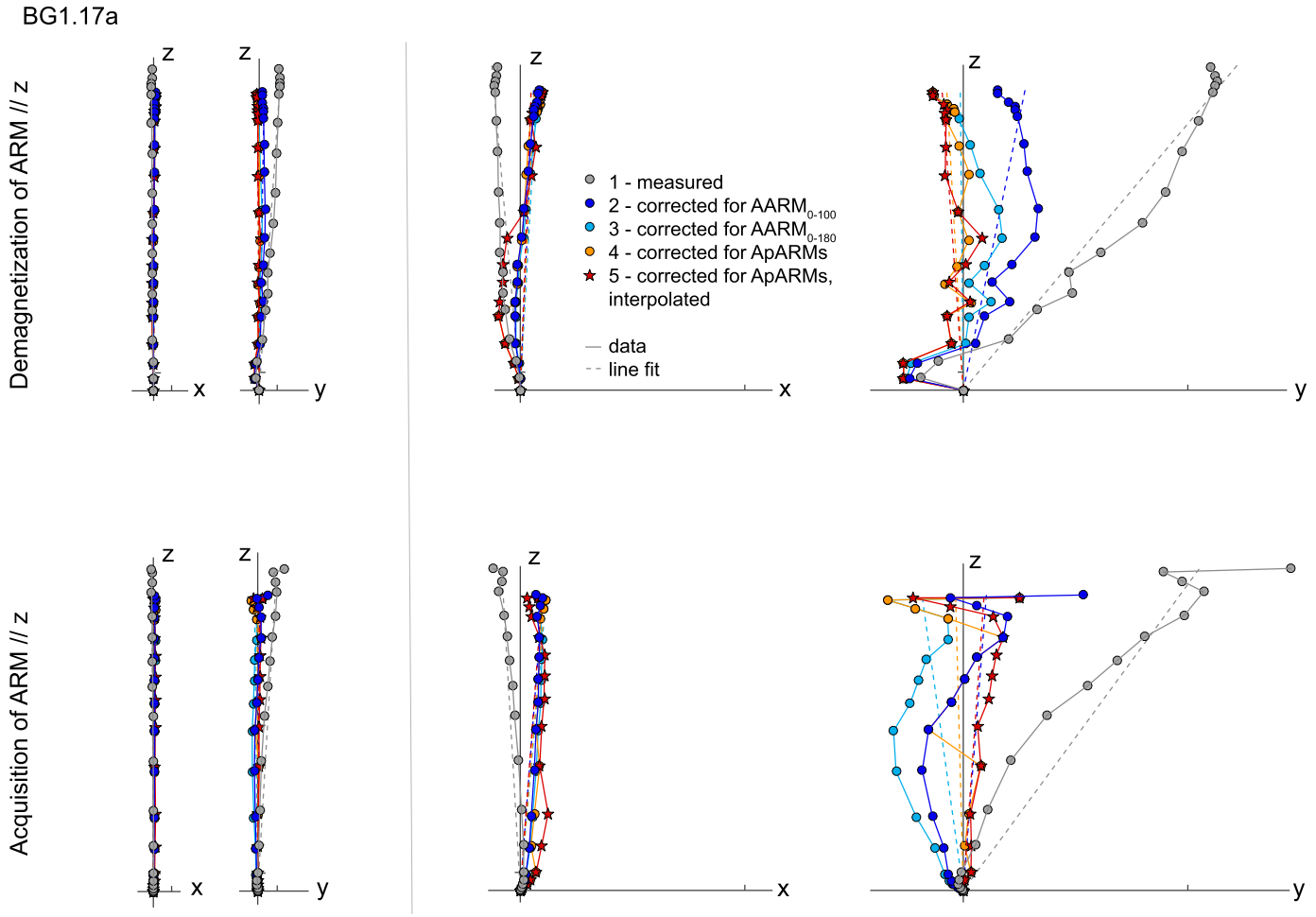

Fig. 7. Vector endpoint diagrams for BG1.17a for demagnetization and acquisition of an ARM parallel to z as measured, and after different types of anisotropy corrections. Vector endpoint diagrams are shown with equal axes (left) and an expanded horizontal axis (right), and tick marks indicate a magnetization of $1 * 10^{-4}$ A m^2/kg.

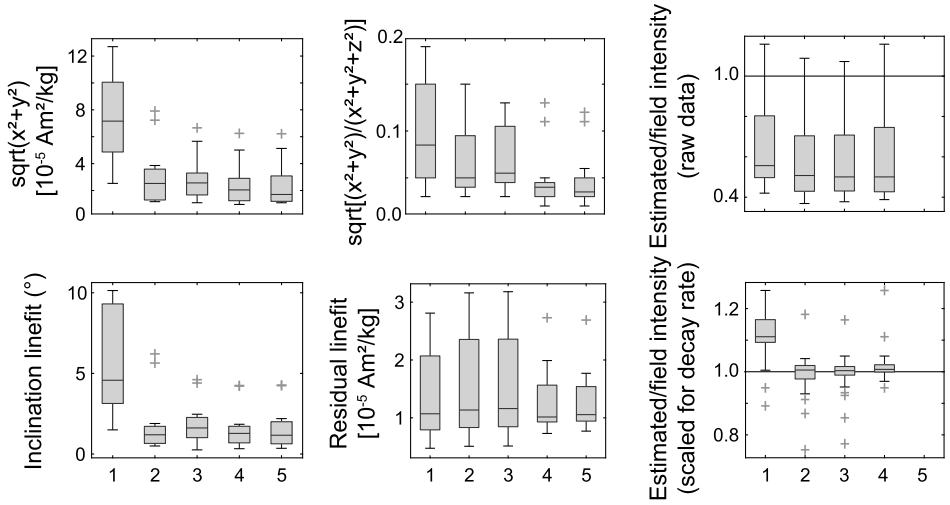

Fig. 8. Error in direction and intensity after different anisotropy corrections. (1) Isotropic correction with mean ARM susceptibility, (2) anisotropy correction with the $AARM_{0–100}$ tensor, (3) anisotropy correction with the $AARM_{0–180}$ tensor, (4) anisotropy correction based on $ApARM_{0–20}$, $ApARM_{20–50}$, $ApARM_{50–100}$ and $ApARM_{100–180}$, correcting all the measurements between 0–20 mT AF for $ApARM_{20–180}$, between 20–50 mT AF for $ApARM_{50–180}$, etc., and (5) interpolated anisotropy correction based on $ApARM_{0–20}$, $ApARM_{20–50}$, $ApARM_{50–100}$ and $ApARM_{100–180}$, correcting the measurements between 0–20 mT AF for $ApARM_{20–180} + a * ApARM_{0–20}$, etc. The reader is referred to the online supplementary for a discussion on the effect of decay rates on the intensity estimates. Boxplots include ARM demagnetization and ARM acquisition for 8 specimens and 19 steps each for directions, and demagnetization and acquisition for 8 specimens and 4 steps for intensities.

$AARM_{0-180}$ than for the isotropic correction. This indicates that for some specimens, anisotropy corrections based on an overall AARM may result in worse estimates of the paleofield direction than if the data was not corrected. Many specimens show little variation between the corrections (2), (3) and (4), however, for some $\sqrt{(M_x^2+M_y^2)/(M_x^2+M_y^2+M_z^2)}$ markedly decreases from (2)/(3) to (4)/(5). Similar observations can be made based on the inclination of the best-fit lines with respect to field direction. Hence, whereas the type of correction may not have much influence on the estimated field direction for the majority of specimens, for some specimens determining individual ApARMs and adding parts of all ApARMs that may contribute significantly improves anisotropy corrections as compared to the integrated $AARM_{0-100}$ or $AARM_{0-180}$.

The reliability of intensity estimates was characterized by the ratio of estimated intensity and known field intensity, for the ARM at fields 0, 20, 50, 100 and 180 mT AF. Hence, only corrections (1)–(4) were calculated. The ratio is generally closer to 1 for corrections (2)–(4) than the isotropic correction (1). Similar as for the estimate of directions, the changes between (2)/(3) and (4) are generally small, but for some specimens, the bulk AARM corrections (2) or (3) result in larger deviations from the known intensity than the uncorrected data, or after correction with individual tensors. Hence, the error in estimated intensity may increase for an anisotropy correction based on a bulk AARM as compared to a paleointensity estimate assuming the specimen is isotropic. For these specimens, the accuracy of intensity estimates significantly increases when the anisotropy corrections are based on a set of individual ApARMs. Note that intensity estimates can additionally be affected by decay rate effects, if the A(p)ARM and ARM demagnetization/acquisition experiments were performed on different instruments (cf. Fig. A, online supplementary for a thorough discussion of this effect).

5.3. Implications for anisotropy corrections in future studies

The results presented here suggest that for rocks with complex remanence anisotropies, it may be necessary to use anisotropy corrections based on a combination of ApARMs rather than a single AARM tensor. More work will be needed to determine whether the same is true for ATRMs, or if anisotropy of TRM behaves differently. By analogy, it is possible that ATRM varies with the temperature interval over which TRMs are imparted. Future studies should investigate this effect, and relate the temperature-dependence of ATRM to the direction of pTRMs acquired in paleointensity studies. A potential challenge with this type of investigation is that each heating step increases the risk of specimen alteration.

Whether or not these more advanced ARM anisotropy corrections are needed depends on the remanence carriers and their fabrics, particularly the interplay of their individual anisotropies. In specimens with a single remanence carrier and a single fabric, remanence anisotropy likely does not depend on coercivity, and therefore a simple correction may be sufficient. On the contrary, in rocks with multiple remanence carriers and complex fabrics, the interplay of individual anisotropies may call for a more advanced anisotropy correction. Coercivity-dependent changes in remanence anisotropy should be checked for in all rocks with complex fabrics of remanence-carrying minerals, because it is not clear *a priori* how the individual fabrics interact and if a more advanced anisotropy correction is necessary.

6. Conclusions and suggestions for future studies

Remanence anisotropy affects both the direction and intensity of magnetization, and may need to be corrected for in paleomagnetic and paleointensity studies. Previous work has highlighted the importance of isolating the anisotropy of the remanence-carrying grains prior to anisotropy corrections, when anisotropy and remanence are carried by different minerals (Bilardello and Kodama, 2010; Selkin et al., 2000). Here, we expand these findings to rocks with multiple remanence and anisotropy carriers, and illustrate how grain-size dependent anisotropies and fabrics affect magnetization. When A(p)ARM varies with coercivity or grain size, this variation can lead to a seemingly multi-component magnetization, even if a specimen is magnetized in a single event and constant field. This study further shows how anisotropy corrections can be adapted in rocks with multiple remanence carriers with distinct fabrics. We suggest that these procedures are applied in future studies, rather than the traditional correction for the bulk anisotropy in a specimen, if specimens contain multiple remanence carriers with different fabrics. More work will be needed to determine whether similar effects are observed for A(p)TRMs acquired over different temperature intervals.

A simple initial test whether remanence anisotropy is coercivity dependent can be done based on directions of ARM imparted in a known field. This test is convenient because ARM acquisition or ARM demagnetization are commonly measured anyway in paleomagnetic studies. Systematic changes in ARM direction with AF step indicate changes in remanence anisotropy. A more complete assessment can be reached by determining ApARMs for different coercivity windows.

Finally, the results presented here indicate that AARM tensors and hence anisotropy corrections are dependent on the experimental parameters that were used when the remanence anisotropy was measured. In addition to the coercivity-dependence, we find a strong variation between mean ARMs acquired on different instruments. We therefore encourage researchers to report all experimental parameters, particularly coercivity window and decay rate that were used to impose ARMs, in future studies.

Acknowledgements

This project was funded by the Swiss National Science Foundation (SNSF), project 167608. The IRM is a US National Multi-user Facility supported through the Instrumentation and Facilities program of the National Science Foundation, Earth Sciences Division (grants 1642268 and 1339505), and by funding from the University of Minnesota. Ken Kodama is thanked for his detailed and thoughtful review. Collection of the specimens from the Bushveld Complex was supported by NSF-EAR 0309686 awarded to Paul Renne and Gary Scott. LT acknowledges support from the National Science Foundation under Grant No. 1547263. This is IRM publication #1802. Data can be obtained from the Supplementary Material of this paper.

Appendix A. Supplementary material

Supplementary material related to this article can be found online at https://doi.org/10.1016/j.epsl.2019.01.051.

References

Aubourg, C., Robion, P., 2002. Composite ferromagnetic fabrics (magnetite, greigite) measured by AMS and partial AARM in weakly strained sandstones from western Makran, Iran. Geophys. J. Int. 151, 729–737.

Ben-Yosef, E., Tauxe, L., Levy, T.E., 2010. Archaeomagnetic dating of copper smelting site F2 in the Timna Valley (Israel) and its implications for the modelling of ancient technological developments. Archaeometry 52, 1110–1121.

Biggin, A.J., Piispa, E.J., Pesonen, L.J., Holme, R., Paterson, G.A., Veikkolainen, T., Tauxe, L., 2015. Palaeomagnetic field intensity variations suggest Mesoproterozoic inner-core nucleation. Nature 526, 245–248.

Biggin, A.J., Steinberger, B., Aubert, J., Suttie, N., Holme, R., Torsvik, T.H., van der Meer, D.G., van Hinsbergen, D.J.J., 2012. Possible links between long-term geomagnetic variations and whole-mantle convection processes. Nat. Geosci. 5, 526–533.

Bilardello, D., Jackson, M.J., 2014. A comparative study of magnetic anisotropy measurement techniques in relation to rock-magnetic properties. Tectonophysics 629, 39–54.
Bilardello, D., Kodama, K.P., 2010. A new inclination shallowing correction of the Mauch Chunk Formation of Pennsylvania, based on high-field AIR results: implications for the Carboniferous North American APW path and Pangea reconstructions. Earth Planet. Sci. Lett. 299, 218–227.
Borradaile, G.J., Almqvist, B.S., 2008. Correcting distorted paleosecular variation in late glacial lacustrine clay. Phys. Earth Planet. Inter. 166, 30–43.
Borradaile, G.J., Lagroix, F., Trimble, D., 2001. Improved isolation of archeomagnetic signals by combined low temperature and alternating field demagnetization. Geophys. J. Int. 147, 176–182.
Bowles, J., Gee, J.S., Kent, D.V., Bergmanis, E., Sinton, J., 2005. Cooling rate effects on paleointensity estimates in submarine basaltic glass and implications for dating young flows. Geochem. Geophys. Geosyst. 6, Q07002.
Buffett, B.A., 2003. The thermal state of Earth's core. Science 299, 1675–1677.
Cisowski, S.M., Collinson, D.W., Runcorn, S.K., Stephenson, A., Fuller, M., 1983. A review of lunar paleointensity data and implications for the origin of lunar magnetism. J. Geophys. Res., Solid Earth 88, A691–A704.
Coe, R.S., 1967. The determination of paleo-intensities of the Earth's magnetic field with emphasis on mechanisms with could cause non-ideal behavior in Thellier's method. J. Geomagn. Geoelectr. 19, 157–179.
Cottrell, R.D., Tarduno, J.A., 1999. Geomagnetic paleointensity derived from single plagioclase crystals. Earth Planet. Sci. Lett. 169, 1–5.
Dietz, R.S., Holden, J.C., 1970. Reconstruction of Pangea: breakup and dispersion of continents, Permian to present. J. Geophys. Res. 75, 4939–4956.
Dunlop, D.J., Schmidt, P.W., Özdemir, Ö., Clark, D.A., 1997. Paleomagnetism and paleothermometry of the Sydney Basin, 1, thermoviscous and chemical overprinting of the Milton Monzonite. J. Geophys. Res. 102, 27285–27295.
Elmore, R.D., Muxworthy, A.R., Aldana, M., 2012. Remagnetization and chemical alteration of sedimentary rocks. In: Elmore, R.D., Muxworthy, A.R., Aldana, M.M., Mena, M. (Eds.), Remagnetization and Chemical Alteration of Sedimentary Rocks. In: Geological Society, London, Special Publications, vol. 371.
Evans, M.E., 1976. Test of the dipolar nature of the geomagnetic field throughout Phanerozoic time. Nature 262, 676–677.
Feinberg, J.M., Scott, G.R., Renne, P.R., Wenk, H.-R., 2005. Exsolved magnetite inclusions in silicates: features determining their remanence behavior. Geology 33, 513.
Feinberg, J.M., Wenk, H.-R., Scott, G.R., Renne, P.R., 2006. Preferred orientation and anisotropy of seismic and magnetic properties in gabbronorites from the Bushveld layered intrusion. Tectonophysics 420, 345–356.
Gattacceca, J., Rochette, P., Bourot-Denise, M., 2003. Magnetic properties of a freshly fallen LL ordinary chondrite: the Bensour meteorite. Phys. Earth Planet. Inter. 140, 343–358.
Hale, C.J., 1987. Palaeomagnetic data suggest link between the Archaean–Proterozoic boundary and inner-core nucleation. Nature 329, 233–237.
Hattingh, P.J., 1986. The palaeomagnetism of the Main Zone in the western Bushveld Complex. Earth Planet. Sci. Lett. 79, 441–452.
Hext, G.R., 1963. The estimation of second-order tensors, with related tests and designs. Biometrika 50 (3/4), 353–373.
Hospers, J., van Andel, S.I., 1969. Palaeomagnetism and tectonics: a review. Earth-Sci. Rev. 5, 5–44.
Irving, E., 1957. Rock magnetism: a new approach to some palaeogeographic problems. Adv. Phys. 6, 194–218.
Jackson, M., Gruber, W., Marvin, J., Banerjee, S.K., 1988. Partial anhysteretic remanence and its anisotropy: applications and grainsize-dependence. Geophys. Res. Lett. 15, 440–443.
Jackson, M.J., Banerjee, S.K., Marvin, J.A., Lu, R., Gruber, W., 1991. Detrital remanence, inclination errors, and anhysteretic remanence anisotropy: quantitative model and experimental results. Geophys. J. Int. 104, 95–103.
Kent, D.V., Irving, E., 2010. Influence of inclination error in sedimentary rocks on the Triassic and Jurassic apparent pole wander path for North America and implications for Cordilleran tectonics. J. Geophys. Res., Solid Earth 115.
Kodama, K.P., 1997. A successful rock magnetic technique for correcting paleomagnetic inclination shallowing: case study of the Nacimiento Formation, New Mexico. J. Geophys. Res., Solid Earth 102, 5193–5205.
Kodama, K.P., 2012. Paleomagnetism of Sedimentary Rocks. Wiley–Blackwell, Chichester, UK. 157 pp.
Kodama, K.P., Dekkers, M.J., 2004. Magnetic anisotropy as an aid to identifying CRM and DRM in red sedimentary rocks. Stud. Geophys. Geod. 48, 747–766.
Letts, S., Torsvik, T.H., Webb, S.J., Ashwal, L.D., 2009. Palaeomagnetism of the 2054 Ma Bushveld Complex (South Africa): implications for emplacement and cooling. Geophys. J. Int. 179, 850–872.
Levi, S., 1977. The effect of magnetite particle size on paleointensity determinations of the geomagnetic field. Phys. Earth Planet. Inter. 13, 245–259.
Mitra, R., Tauxe, L., McIntosh, S.K., 2013. Two thousand years of archeointensity from West Africa. Earth Planet. Sci. Lett. 364, 123–133.
Morel, P., Irving, E., 1981. Paleomagnetism and the evolution of Pangea. J. Geophys. Res., Solid Earth 86, 1858–1872.
Pesonen, L.J., Nevanlinna, H., 1981. Late Precambrian Keweenawan asymmetric reversals. Nature 294, 436–439.
Potter, D.K., 2004. A comparison of anisotropy of magnetic remanence methods – a user's guide for application to paleomagnetism and magnetic fabric studies. In: Martín-Hernández, F., Lüneburg, C.M., Aubourg, C., Jackson, M. (Eds.), Magnetic Fabrics: Methods and Applications. The Geological Society, London, UK, pp. 21–35.
Prévot, M., Mankinen, E.A., Coe, R.S., Grommé, C.S., 1985. The Steens Mountain (Oregon) geomagnetic polarity transition: 2. Field intensity variations and discussion of reversal models. J. Geophys. Res., Solid Earth 90, 10417–10448.
Rogers, J., Fox, J.M.W., Aitken, M.J., 1979. Magnetic anisotropy in ancient pottery. Nature 277 (5698), 644–646.
Selkin, P.A., Gee, J.S., Tauxe, L., 2007. Nonlinear thermoremanence acquisition and implications for paleointensity data. Earth Planet. Sci. Lett. 256, 81–89.
Selkin, P.A., Gee, J.S., Tauxe, L., Meurer, W.P., Newell, A.J., 2000. The effect of remanence anisotropy on paleointensity estimates: a case study from the Archean Stillwater Complex. Earth Planet. Sci. Lett. 183, 403–416.
Selkin, P.A., Gee, J.S., Meurer, W.P., Hemming, S.R., 2008. Paleointensity record from the 2.7 Ga Stillwater Complex, MT. Geochem. Geophys. Geosyst. 9, Q12023. https://doi.org/10.1029/2008GC001950.
Shaar, R., Tauxe, L., 2013. Thellier GUI: an integrated tool for analyzing paleointensity data from Thellier-type experiments. Geochem. Geophys. Geosyst. 14. https://doi.org/10.1002/ggge.20062.
Smirnov, A.V., Kulakov, E.V., Foucher, M.S., Bristol, K.E., 2017. Intrinsic paleointensity bias and the long-term history of the geodynamo. Sci. Adv. 3, e1602306.
Stephenson, A., Sadikun, S., Potter, D.K., 1986. A theoretical and experimental comparison of the anisotropies of magnetic susceptibility and remanence in rocks and minerals. Geophys. J. R. Astron. Soc. 84, 185–200.
Stillinger, M.D., Hardin, J.W., Feinberg, J.M., Blakely, J.A., 2016. Archaeomagnetism as a complementary dating technique to address the Iron Age chronology debate in the Levant. Near East. Archaeol. 79, 90–106.
Swanson-Hysell, N.L., Maloof, A.C., Weiss, B.P., Evans, D.A.D., 2009. No asymmetry in geomagnetic reversals recorded by 1.1-billion-year-old Keweenawan basalts. Nat. Geosci. 2, 713–717.
Tarduno, J.A., Cottrell, R.D., Smirnov, A.V., 2006. The paleomagnetism of single crystals: recording geomagnetic field strength during mixed polarity intervals, superchrons, and inner core growth. Rev. Geophys. 44.
Tauxe, L., Kent, D.V., 2004. A simplified statistical model for the geomagnetic field and the detection of shallow bias in paleomagnetic inclinations: was the ancient magnetic field dipolar? In: Geophysical Monograph Series, vol. 145.
Tauxe, L., Yamazaki, T., 2015. Paleointensities. 2nd edition. In: Schubert, Gerald (Ed.), Treatise on Geophysics, vol. 5. Elsevier, Oxford, pp. 461–509.
Tema, E., 2009. Estimate of the magnetic anisotropy effect on the archaeomagnetic inclination of ancient bricks. Phys. Earth Planet. Inter. 176, 213–223.
Trindade, R.I.F., Raposo, M.I.B., Ernesto, M., Siqueira, R., 1999. Magnetic susceptibility and partial anhysteretic remanence anisotropies in the magnetite-bearing granite pluton of Tourao, NE Brazil. Tectonophysics 314, 443–468.
van der Voo, R., Torsvik, T.H., 2001. Evidence for late Paleozoic and Mesozoic nondipole fields provides and explanation for the Pangea reconstruction problems. Earth Planet. Sci. Lett. 187, 71–81.
Walton, D., 1980. Time-temperature relations in the magnetization of assemblies of single domain grains. Nature 286, 245–247.
Watson, G.S., 1983. Large sample theory of the Langevin distribution. J. Stat. Plan. Inference 8, 245–256.
Yu, Y., 2011. Importance of cooling rate dependence of thermoremanence in paleointensity determination. J. Geophys. Res. 116, B09101. https://doi.org/10.1029/2011JB008388.
Yu, Y., Tauxe, L., Genevey, A., 2004. Toward an optimal geomagnetic field intensity determination technique. Geochem. Geophys. Geosyst. 5, Q02H07. https://doi.org/10.1029/2003GC000630.